Coastal Engineering, 8 (1984) 73—93
Elsevier Science Publishers B.V., Amsterdam — Printed in The Netherlands

PERFORMANCE OF A NUMERICAL SHORT-WAVE MODEL

P.A. MADSEN and I.R. WARREN

Danish Hydraulic Institute, Agern Alle 5, DK-2970 Horsholm (Denmark)

(Received January 18, 1983; revised and accepted May 9, 1983)

ABSTRACT

Madsen, P.A. and Warren, I.R., 1984. Performance of a numerical short-wave model. Coastal Eng., 8: 73—93.

A numerical short-wave model system based on the Boussinesq equations is verified against analytical as well as experimental results for shoaling, refraction, diffraction and partial reflection processes. It is shown that engineers can confidently and responsibly apply such a model system to the study of wave disturbance in coastal regions.

INTRODUCTION

In order to provide an assessment of the wave conditions in existing or proposed new harbours, a detailed knowledge of the directions of propagation and of the magnitudes of the transmitted waves is required.

For this purpose mathematical short-wave models have been applied in engineering practise. These models can simulate water level variations and flows in estuaries, bays and coastal areas, including short-wave phenomena.

The model systems considered here are based on the time-dependent vertically integrated Boussinesq equations of conservation of mass and momentum (shown in Appendix A), and are able to simulate unsteady two-dimensional flows in vertically homogeneous fluids. The inclusion of Boussinesq terms is of particular importance to the short-wave simulations. These terms account for the deviation from hydrostatic pressure distribution due to the vertical accelerations, and make it possible to consider a large range of water waves which are not restricted by linear assumptions. Furthermore, the equations include porosity which makes it possible to simulate partial reflection from piers and breakwaters. The particular numerical model used in the study presented here is described in detail by Abbott et al. (1978, 1983).

The transmission of waves from the sea into a harbour protected by breakwaters is a process which involves shoaling, refraction, diffraction and reflection processes.

This paper will present comparisons between model simulations of these

0378-3839/84/$03.00

processes and analytical solutions as well as physical model tests. It will prove that engineers can confidently apply such models to the study of development projects for harbours and coastal regions.

First one-dimensional shoaling tests are compared against experimental data of surface profiles and wave heights up to breaking. Secondly, a solution provided by the modelling system is compared to a theoretical solution for depth refraction of cnoidal waves over straight and parallel sea-bed contours given by Skovgaard and Petersen (1977).

Theoretical solutions for diffraction around a single, fully reflecting breakwater are given in the Shore Protection Manual. Comparison is made with these solutions for the case of a 45 degrees and a 90 degrees diffraction. Furthermore, the model is verified against theoretical solutions for diffraction around an absorbing breakwater.

Reflection and transmission from vertical porous structures were solved analytically by Madsen and White (1976) for the case of linear shallow-water waves. The modelling system results are compared to these results and to the experiments of Keulegan (1973).

Finally, numerical model tests with wave absorbers have been made. The computational results are compared to an analytical solution by Madsen (1983) and a qualitative comparison is made with the measurements by Straub (1956).

SHOALING

One-dimensional computational shoaling tests have been carried out, simulating the behaviour of periodic waves up to breaking point. Bottom friction is included in the modelling and comparison is made with experimental data obtained at CERC and Delft laboratories (Singamsetti and Wind, 1980; see Table I for details). A Chezy type of bottom friction has been applied in the computations:

$$\tau = \frac{\rho g}{C^2} U|U|, \quad C \text{ constant} \tag{1}$$

The optimum value of C for each of the two experiments has been chosen by trial-and-error, and the resulting comparisons are shown in Figs. 1 and 2.

An excellent agreement with the measurements from CERC can be obtained with a Chezy number of 20 (Fig. 1). However, using the same Chezy number for the comparison with the experiments from Delft yields an underestimation of the wave height near the breaking point. Instead, satisfactory agreement is obtained with a Chezy number of 30. Notice that the computed wave heights are sensitive to the choice of C only from the toe of the slope up to the breaking point (Fig. 2).

In order to justify the present choices of the Chezy number, eq. 1 is compared with a more precise description of the bottom friction:

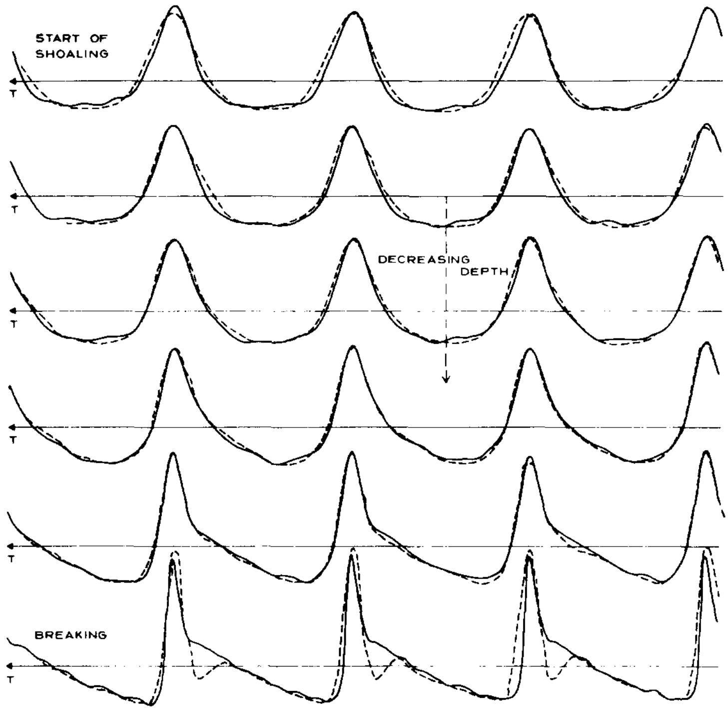

Fig. 1. Shoaling wave comparison in surface profiles.
Solid line = physical model (CERC); dashed line = numerical model; T = 4 s; H_0 = 0.14 m; h_0 = 0.6 m.

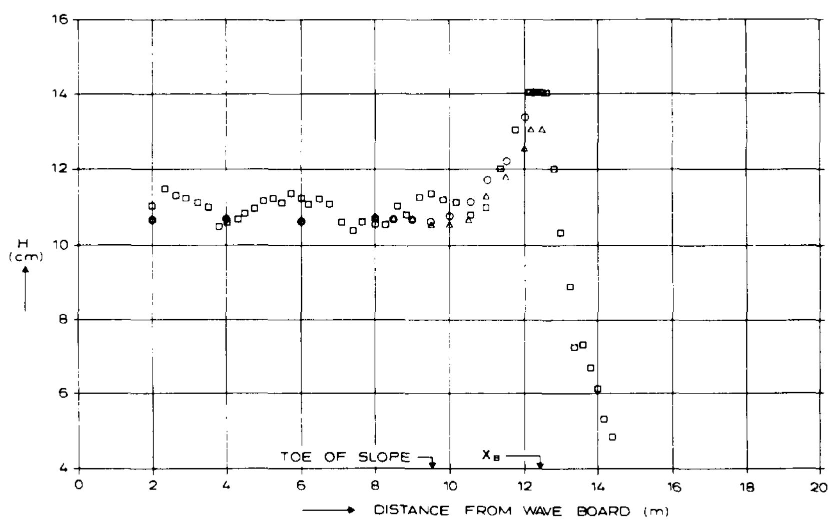

Fig. 2. Shoaling wave comparison in wave heights. Circles = numerical model, CHEZY = 30; triangles = numerical mode, CHEZY = 20; squares = experiments from Delft Hydraulics Laboratory; T = 1.55 s; H_0 = 0.11 m; h_0 = 0.30 m.

$$\tau = \tfrac{1}{2} \rho f_w U|U| \tag{2}$$

where f_w is a function of the particle motion amplitude α and of the Nikuradse roughness k_N. Laboratory measurements by Jonsson (1976) showed that f_w can be determined from:

$$f_w = 0.30 \quad \text{for} \quad \frac{\alpha}{k_N} < 1.57 \tag{3}$$

$$\frac{1}{4\sqrt{f_w}} + \log \frac{1}{4\sqrt{f_w}} = -0.08 + \log \frac{\alpha}{k_N} \quad \text{for} \quad \frac{\alpha}{k_N} > 1.57$$

The Nikuradse roughness parameter is defined from the velocity distribution in a steady, turbulent uniform flow over a rough bed. Hence k_N is not a function of the wave parameters but merely a function of the bottom material. However, the width of the channel may be important as the friction along the sides of the channel will tend to increase f_w, i.e. to increase k_N.

Comparing eqs. 1, 2 and 3 makes it possible to relate the chosen values of C to values of α/k_N. C equal to 20 yields α/k_N = 18.2 and C equal to 30 yields α/k_N = 100. Now using sinusoidal theory allows for an approximate

TABLE I

Characteristics in shoaling experiments

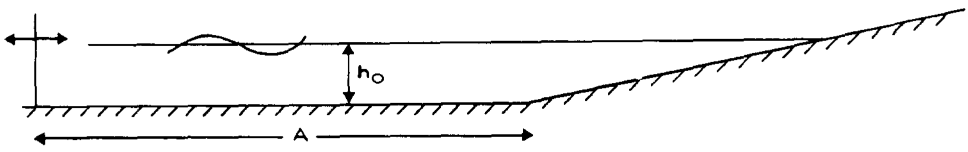

	Delft	CERC
A (m)	9.80	22.0
width (m)	1.13	0.46
slope	1/20	1/30
T (sec)	1.55	4.1
h_0 (m)	0.30	0.60
H_0 (m)	0.11	0.13
L_0 (m)	2.4	9.7
α_0 (m)	0.07	0.17
h_b (m)	0.17	0.23
H_b (m)	0.14	0.20
L_b (m)	$\approx$1.9	$\approx$6.0
α_b (m)	$\approx$0.12	$\approx$0.42

solution for α at the toe of the slope as well as at the breaking point. Hence the chosen values of C can be related to a range of corresponding k_N values.

From the CERC measurements α can be determined to be 0.18 m and 0.42 m at the toe of the slope and at the breaking point respectively. With C equal to 20 $m^{1/2}$ s^{-1} this leads to k_N values in the range of 9—23 mm.

From the Delft measurements α can be determined to be 0.07 m and 0.13 m at the toe of the slope and at the breaking point respectively. Hence with C equal to 30 $m^{1/2}$ s^{-1} this yields k_N in the range of 0.7—1.3 mm.

The differences in roughness parameters in the two experiments are obviously rather large but may be justified by the differences in model setup: The Delft measurements were performed in a very smooth channel with water depth 0.30 m and width equal to 1.13 m while the CERC measurements were performed with water depth 0.60 m and width equal to 0.46 m. Hence, the friction from the sidewalls cannot be neglected in the CERC measurements which probably explains the higher k_N values in this case.

It can be concluded that satisfactory shoaling computations can be made by using the simple Chezy formula. However, in order to determine a reasonable value of C, information is required about the roughness parameter for the specific bed material.

REFRACTION

A theoretical solution for the depth refraction of a first-order cnoidal surface gravity wave in shallow water was given by Skovgaard and Petersen (1977) for a quasi two-dimensional situation, i.e. for a gently sloping bathymetry characterized by straight and parallel sea-bed contours (Fig. 3).

This quasi two-dimensional situation permitted the determination of the wave refraction solution (except for the orthogonal paths) as a function of the depth as the only independent variable without integrating the differential equations for the orthogonal paths.

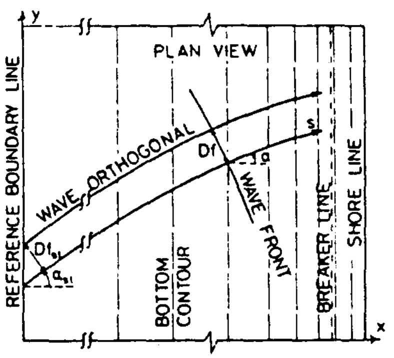

Fig. 3. Definition sketch for refraction over straight and parallel bottom contours.

With the basic assumption that the energy flux is constant between adjacent wave orthogonals, Skovgaard and Petersen derived two non-linear algebraic equations with the wave height and the cnoidal parameter m as unknowns. Sinusoidal and cnoidal theory were matched assuming continuity in the energy flux and accepting the resulting discontinuity in the wave height.

In order to be able to compare the numerical model with the theoretical solutions, we have chosen the top row in table 1 from Skovgaard ands Petersen (1977) as the boundary conditions:

$$\frac{h}{L_0} = 0.045, \quad \frac{H}{h} = 0.0826 \quad \text{and } \alpha_0 = 25.9°$$

where h is the water depth, H the wave height, L_0 the deep-water wave length and α_0 the initial angle of incidence.

Hence, choosing a water depth of 21 m at the open boundary defines the incoming wave height and period as 1.74 m and 17.3 s, respectively.

The model topography is shown in Fig. 4. The angle of incidence, α_0, is

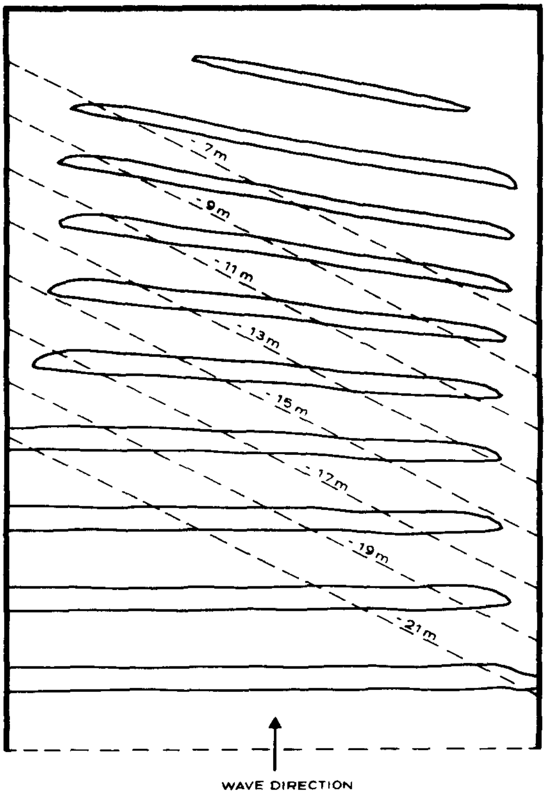

Fig. 4. Refraction of cnoidal waves. Dashed line = bottom contours; solid line = wave fronts computed by numerical model (zero elevation isolines); T = 17 s; H_i = 1.74 m; h = 21 m; $\Delta x = \Delta y$ = 15.5 m; Δt = 1 s.

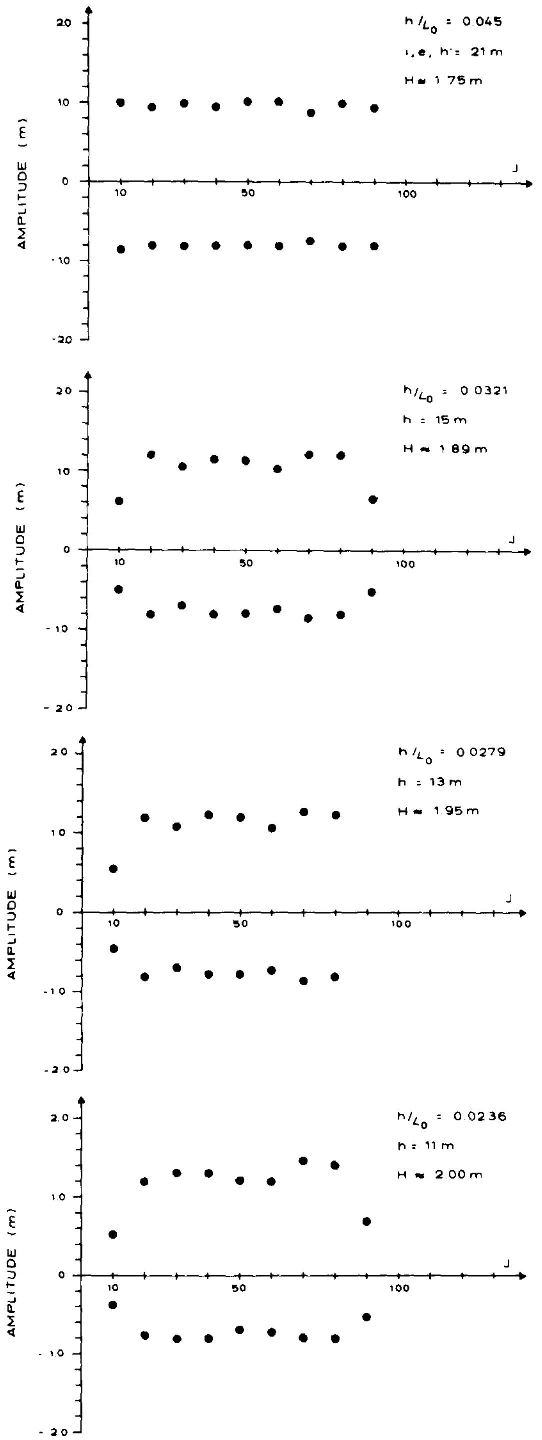

Fig. 5. Computed maximum and minimum surface elevations along a bottom contour.

slightly modified from 25.9° to 26.6°. However, this change is considered to have little impact on the results. The model size is 100 × 140 grid points and in order to have at least 10 grid points per wave length, the grid sizes are $\Delta x = \Delta y = 15.5$ m, while the time step is 1 s. The bottom contours rise from −21 m to −7 m over 70 grid points, leading to a rather flat slope ($h_x \approx 0.013$) which is consistent with the classical shoaling theory.

In order to minimize the reflections from the closed boundaries a porosity filter layer has been applied. This filter layer is discussed further in the section on reflection from a porous wave absorber.

From the isoline plot of the computed wave fronts in Fig. 4 it is noticed that the reflection is indeed very small and no sign of standing waves near the far end of the model can be seen.

From time-series plots of computed surface elevations the time mean values of the maximum and minimum elevations are determined in every 10th grid point along the 21, 19, 17, 15, 13, 11, 9 and 7 m bottom contours (Fig. 5). Firstly, we notice that the maximum and minimum elevations are nearly constant along each bottom contour. This agrees with the theoretical solution which predicts that the refracted wave heights are functions only of the water depth (for given reference waves). However, we do find considerable disturbances, especially in the maximum elevations for $h \leqslant 9$ m. This is to be expected from the truncation errors, which become significant as $\Delta x/h$ increases to 2.2 at $h = 7$ m. At this water depth, secondary waves appear in the wave troughs.

In order to determine a representative wave height occurring along a bottom contour, space mean values are calculated based on the middle area of the model in order to avoid boundary effects. The chosen values are shown on Fig. 5. These values have been compared with the theoretical solution from Skovgaard and Petersen (Table I) and the agreement is indeed very statisfactory (Fig. 6). Finally, the angles of incidence have been determined from the isoline plot of the wave fronts (Fig. 4) and once again the agreement with Table I in Skovgaard and Petersen (1977) is good (Fig. 7).

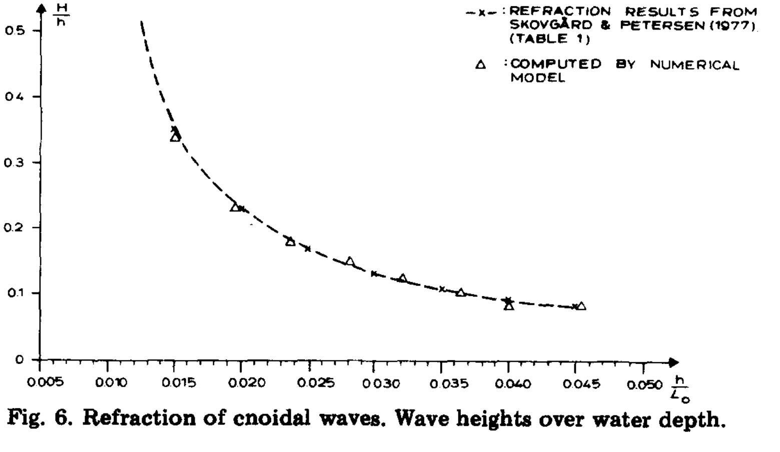

Fig. 6. Refraction of cnoidal waves. Wave heights over water depth.

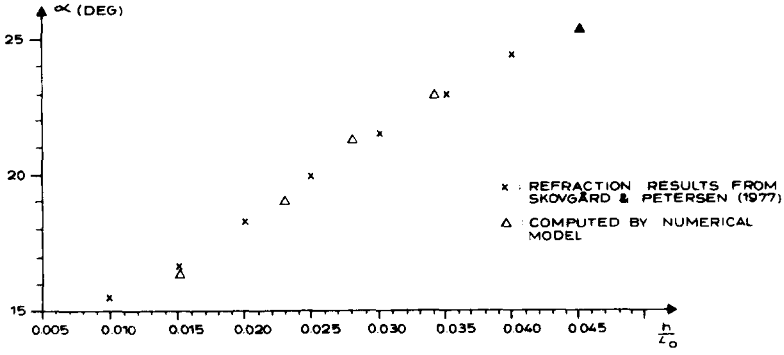

Fig. 7. Refraction of cnoidal waves. Angle of incidence.

DIFFRACTION

A 45° and a 90° diffraction around a single fully reflecting breakwater on a horizontal bottom have been simulated and a comparison has been made with the theoretical solutions from the Shore Protection Manual. Furthermore, computations and theoretical solutions have been compared for the case of a fully absorbing breakwater.

There is a minor problem in performing the comparisons because of the fact that the theoretical solutions and the numerical model are based on two different wave theories. While the numerical model is based on finite difference approximations of the Boussinesq equations, the diffraction curves shown in the Shore Protection Manual are based on solutions of the Sommerfelds equations assuming infinitesimally small water waves (linear wave theory). Hence, although a sinusoidal input would match with the theoretical basis for the curves in the Shore Protection Manual, it will not match with the difference equations and the wave will have to change its form during the propagation in order to adjust itself to the Boussinesq equations.

On the other hand, a cnoidal wave input will not propagate with a constant wave length because of the dependence upon the wave height, and this is also in conflict with the theory.

What we have done is to run the model with a cnoidal input having a very low value of the Ursell parameter:

$$U = HL^2/h^3$$

In this case the differences between the sinusoidal and cnoidal profiles will be moderate. In order to describe a typical wave occurring in harbours, the following choice for the model tests has been made:

h = 10 m (constant depth of the area)
T = 8 s (incoming wave period)
H_i = 2 m (incoming wave height)

Hence, a sinusoidal as well as a cnoidal theory leads to a wave length of approximately 70 m which yields an Ursell parameter of approximately 10.

The grid sizes Δx and Δy are chosen to be 7 m, representing the waves with approximately 10 points per wave length. The time step is chosen to be 0.5 s, representing the waves with 16 points per wave period.

The model size is chosen to be 100 × 100, i.e. approximately 10 wave lengths in each direction and the width of the entrance for the incoming waves is 4 wave lengths (Fig. 8). Reflections from the northern and eastern closed boundaries are minimized by applying an absorbing porosity filter which has the effect of simulating an infinite domain. Reflections from the western closed boundary are expected to be small and have not been treated by a filter. The computational results can be seen in Figs. 8—10.

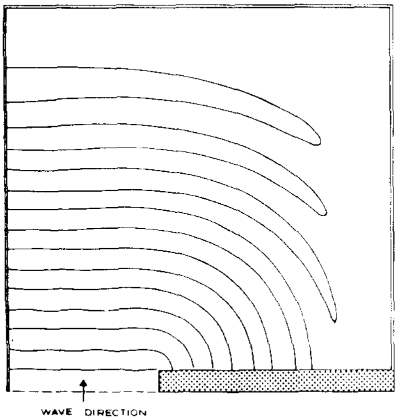

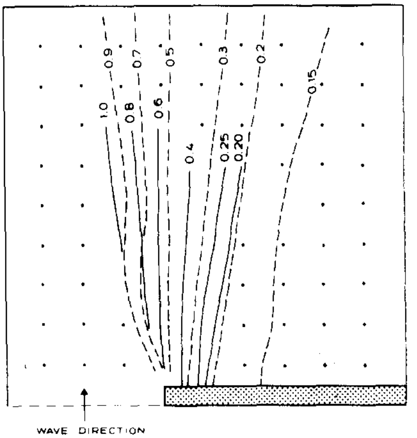

a b

Fig. 8. Diffraction around a fully reflecting breakwater (90°C). a. Isoline plot of wave fronts. b. Wave heights H/H_i. Dashed line = theory from Shore Protection Manual; solid line = computed by numerical model. Cnoidal input, T = 8 2; H_i = 2 m, h = 10 m, Δx = Δy = 7 m, Δt = 0.5 s.

In Fig. 8 a 90° diffraction around a fully reflecting breakwater is shown. The agreement with the Shore Protection Manual is excellent in this case.

In Fig. 9 a 45° diffraction around a fully reflecting breakwater is shown, and once again the agreement is very good in most of the area. However, we do find discrepancies very near the breakwater. These are caused by the boundary formulation in the numerical model, where a solid boundary at 45° to the grid is represented by a number of finite steps (Fig. 9a). It is well-known that reflections from these steps cause errors (in this case an over-estimate of the waves) close to the breakwater.

The effect of the steps can be avoided by applying a porosity layer (discussed below) along the front face of the breakwater. However, this

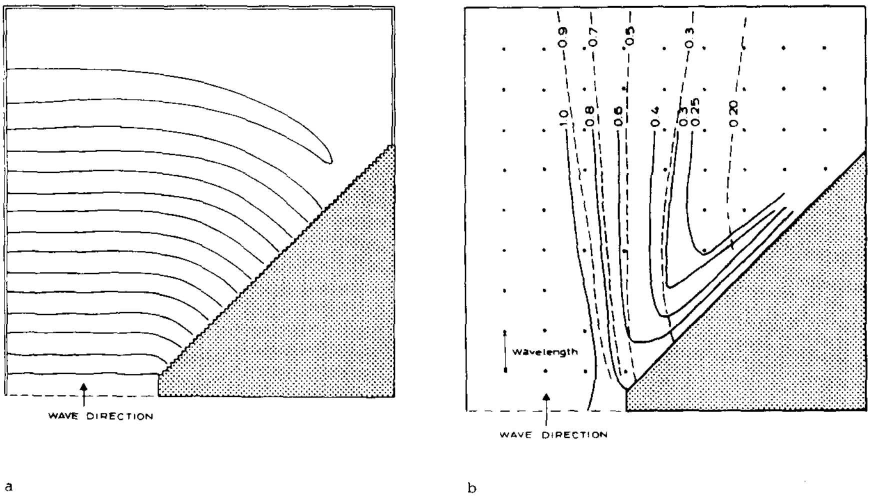

Fig. 9. Diffraction around a fully reflecting breakwater (45°). a. Isoline plot of wave fronts. b. As Fig. 8.

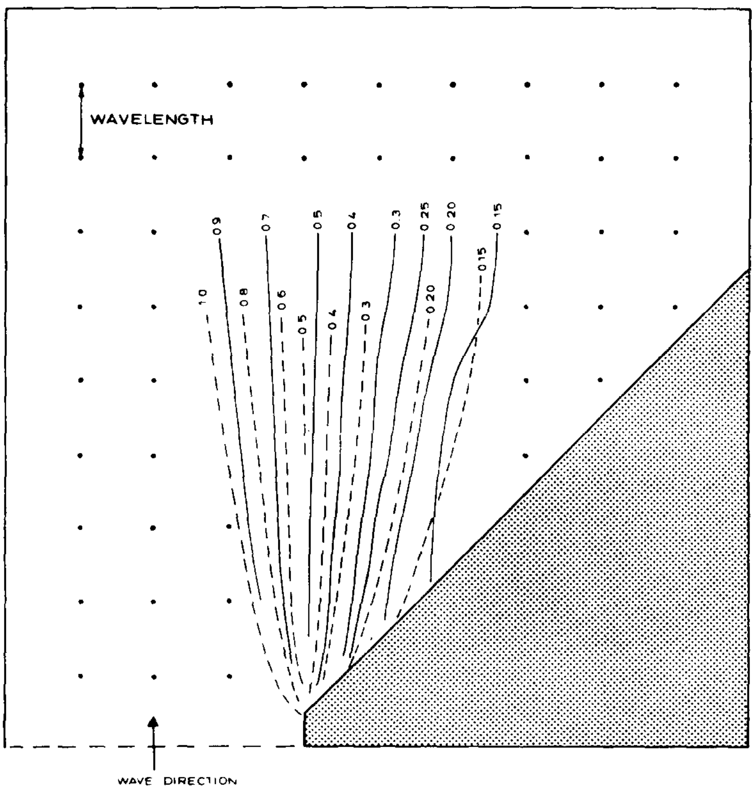

Fig. 10. Diffraction around a fully absorbing breakwater (45°). Wave heights H/H_i. Dashed line = theory; solid line = numerical model (incl. porosity along the breakwater). Input as Fig. 8.

introduces an energy dissipation which will influence the waves not only in the vicinity of the breakwater but in the whole shallow area behind the breakwater.

In Fig. 10 such a solution is compared to the theory of fully absorbing breakwaters. The agreement turns out to be very satisfactory. Hence, we can conclude that although the basis for the theory and the basis for the model runs are different and although we have used an incoming wave as high as 20% of the water depth, the agreement in diffraction coefficients is acceptable in most of the model area. Furthermore, this result indicates that the diffraction process can be considered to be fairly linear with respect to wave height, at least if the area is scaled with respect to the resulting wave length.

REFLECTION AND TRANSMISSION FROM POROUS RUBBLE MOUNDS

In short-wave modelling of harbours it is important to simulate partial reflections from piers and breakwaters. In the model presented here, this is done by including porosity in the conservation equations (Appendix A). The flow resistance inside the porous structures is described by the non-linear term:

$$(\alpha + \beta|U|)U$$

where α and β account for the laminar and turbulent friction loss respectively. α and β are determined by the empirical expressions recommended by Engelund (1953):

$$\alpha = \alpha_0 \frac{(1-n)^3}{n^2} \frac{\nu}{d^2}$$

$$\beta = \beta_0 \frac{(1-n)}{n^3} \frac{1}{d}$$

in which d is the grain size, ν the kinematic viscosity and α_0 and β_0 are constant particle-form coefficients which in the following computations have been taken to be 1000 and 2.8, respectively.

With a porosity less than 1 the flow inside the permeable structure can be simulated. With the porosity equal to 1 the friction loss becomes zero and the equations simplify to the normal Boussinesq equations describing the flow outside the structures.

Small-scale experiments on reflection and transmission characteristics of porous rectangular breakwaters were performed by Keulegan (1973). The numerical model is set up to the same scale as Keulegan's physical model and for comparison purpose we use the experimental data corresponding to relatively long waves ($h/L = 0.1$).

From the specifications of the physical model the water depth, h, is known to be 0.30 m. Hence $h/L = 0.1$ and combining this with sinusoidal theory leads to a wave period $T = 4.86$ s. We regard two different cases, the width of the rubble-mound being equal to 0.15 m and 0.30 m, respectively. The diameter of grains is 0.025 m and the porosity is taken to be 0.46 (see Madsen and White, 1976).

An important parameter in the numerical solution is the grid size of the finite difference scheme. Firstly, it is limited by the width (w) of the rubble-mound, and, secondly, it should not be larger than approximately 1/10 of the wave length, L. In the two cases studied here, W/L takes values of 0.05 and 0.1, respectively, so that the highest values of Δx are 0.15 m and 0.30 m, respectively. Four different values of Δx have been tested in order to investigate how sensitive the results are to this parameter. The timesteps are varied with the gridsizes in such a way that the Courant number:

$$Cr \equiv \frac{L/\Delta x}{T/\Delta t} \approx 1$$

A definition sketch of the model setup is shown in Fig. 11. It should be noted that an absorbing filter is used at the far end of the model in order to minimize any reflection from the closed boundary.

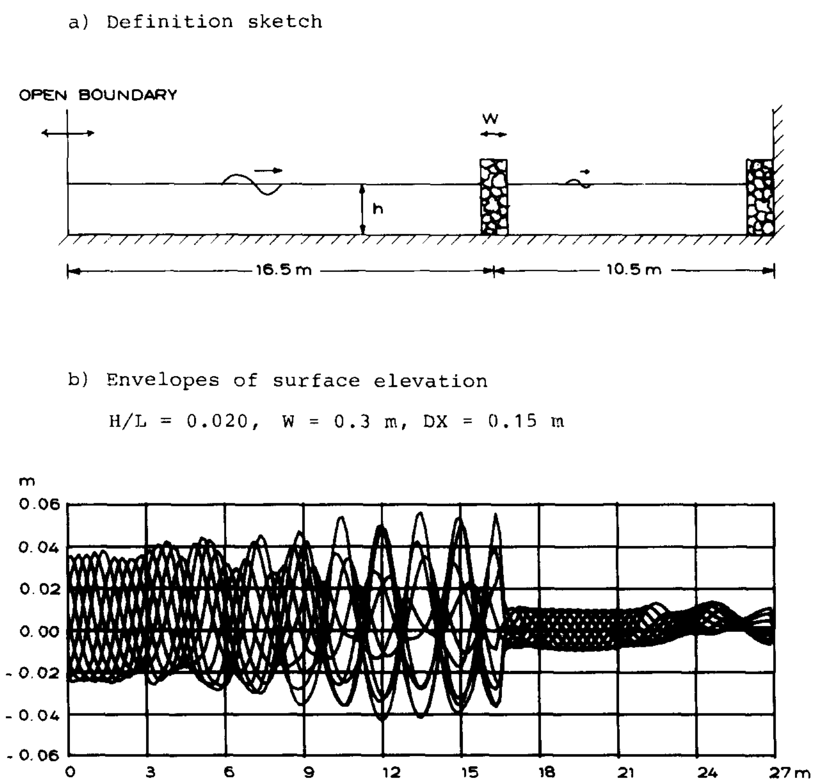

Fig. 11. Transmission through a rubble-mound breakwater.

The computed surface elevations are plotted as a number of line plots during a wave period. These make an envelope of the surface elevations (Fig. 11b) from which the reflection coefficient, α_R, can be determined using Healy's formula:

$$\alpha_R = \frac{a_{max} - a_{min}}{a_{max} + a_{min}}$$

The computed results are tested against the experimental data from Keulegan (1973) in Fig. 12a, b.

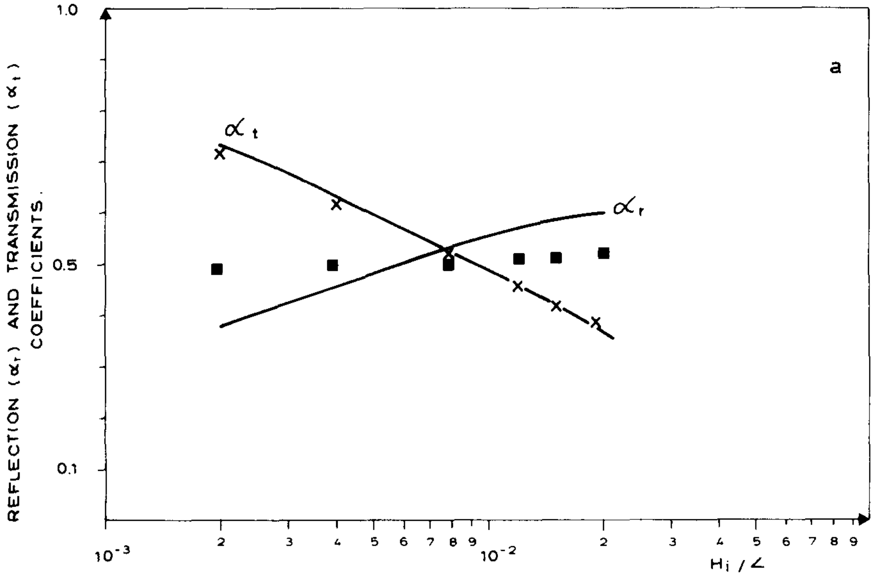

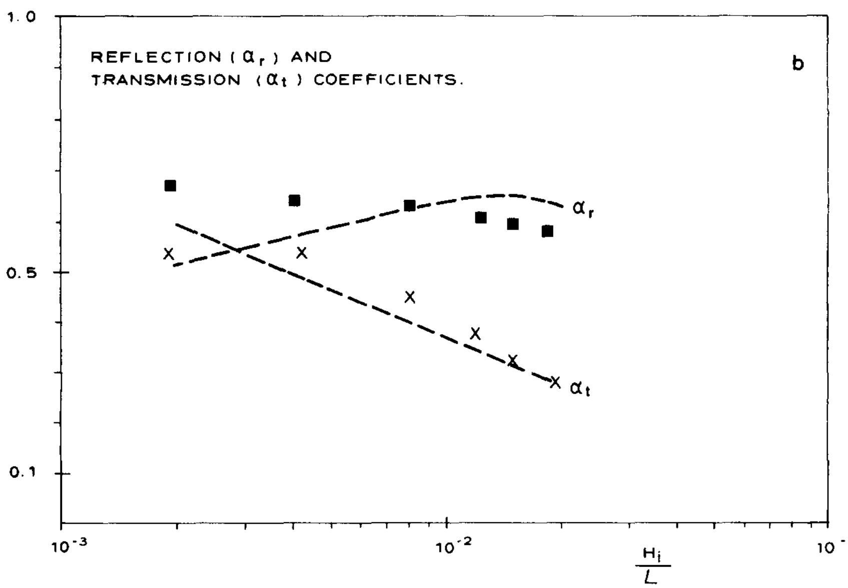

In Fig. 12a the computed transmission coefficients are seen to be in excellent agreement with the experimental ones, whereas the agreement in Fig. 12b leaves something to be desired. However, Madsen and White (1976) found that in order to fit the latter experiments (Fig. 12) they had to use a smaller value of β_0 (= 2.2) while we have used the value 2.8 in all the computations.

Regarding the reflection coefficients in Fig. 12a, b, a significant discrepancy between observation and prediction can be seen. This discrepancy is probably due to experimental errors in the determination of the minimum and maximum wave amplitudes of the wave envelope in the reflected wave region. Madsen and White (1976) showed that the expression for α_R is very sensitive to erroneous results in a_{min} and indeed it is no easy task to determine the exact position of the nodes and anti-nodes in a physical model.

In Fig. 13a the numerical solution is shown for 3 different grid sizes corresponding to $w/\Delta x$ equal to 1, 2 and 4, respectively (w being the width of the rubble-mound).

Obviously $w/\Delta x = 1$ yields too coarse a grid size, leading to an overestimation of the transmission and an underestimation of the reflection.

The differences in using $w/\Delta x = 2$ and 4 are not alarming and there seems to be no reason to represent the rubble-mound with more than 4 grid points. The numerical solution is compared to the theoretical solution made by Madsen and White (1976) and the agreement is very good, especially with respect to the transmission coefficients.

In Fig. 13b the width of the rubble-mound is doubled while the wave input is the same, i.e. for the same value of $w/\Delta x$ the value of $L/\Delta x$ will be different. The result is that $w/\Delta x = 2$ is no longer acceptable and the differences between using $w/\Delta x = 2$ and $w/\Delta x = 4$ has become significant.

On the other hand, there is nearly no difference between using $w/\Delta x = 4$ or 8; hence once again we can conclude that a reasonable representation of a transmitting rubble-mound can be made using 4 grid points.

The agreement with the theoretical solution (Madsen and White, 1976) is still very good although we find some discrepancies in the reflection coefficients. Generally, it can be concluded that the simplifications made by Madsen and White, such as for instance the linearisation of the friction terms in the momentum equation, are reasonable.

Finally, the energy loss within the rubble-mound has been calculated by the expression:

$$\mathrm{DISS} = 1 - (\alpha_t^2 + \alpha_r^2)$$

Fig. 12. Comparison between computed and measured transmission. a. Squares = α_r and crosses = α_t, experimental data, Keulegan (1973). Dashed line = computed (DX = 0.0375 m, DT = 0.025 s). T = 1.86 s, h = 0.3 m, width = 0.15 m, porosity = 0.46. b. Data as in a, but with width = 0.30 m, DX = 0.075 m, DT = 0.050 s.

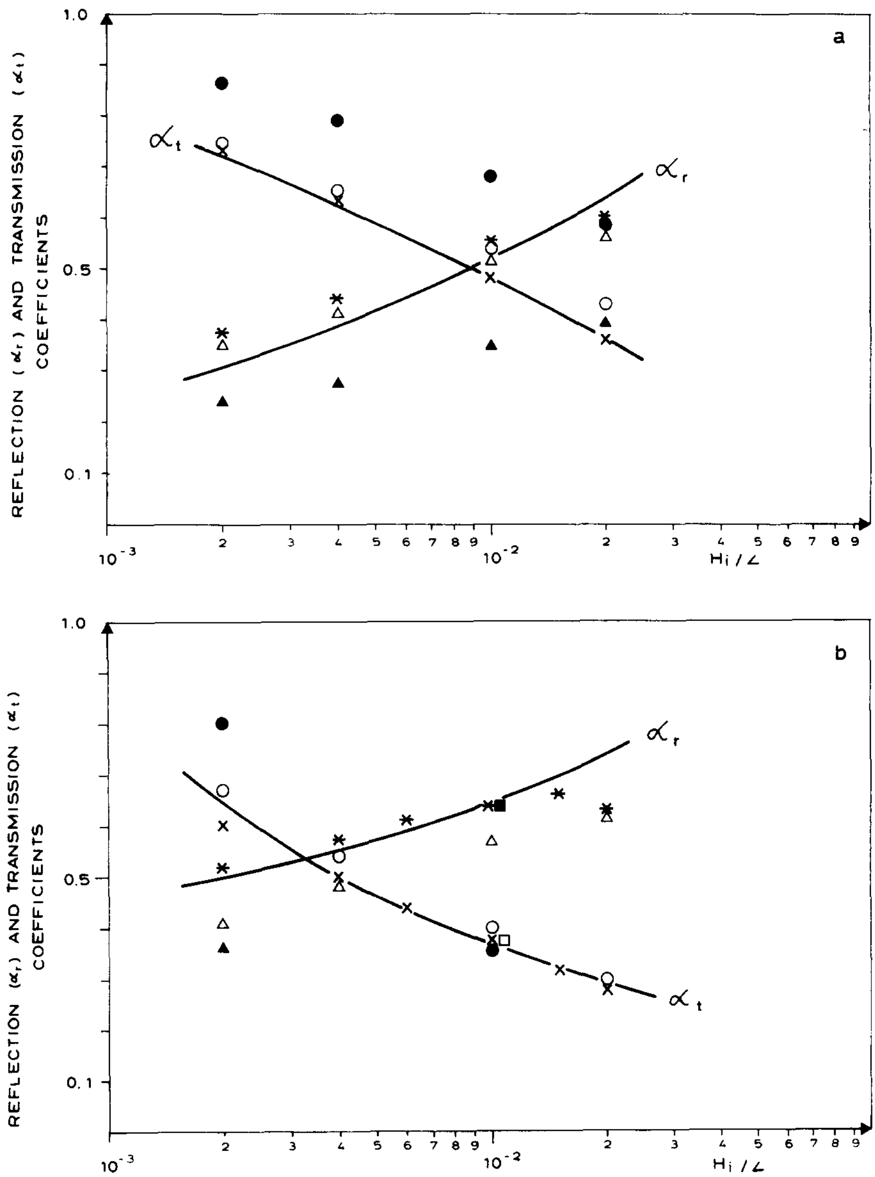

Fig. 13. Comparison between numerical solution and a theoretical solution. a. Data as in Fig. 12a. Solid line = theoretical solution by Madsen and White (1976). α_t, α_r by numerical solution: •, ▲ DX = 0.15 m, DT = 0.10 s; ○, △ DX = 0.075 m, DT = 0.050 s; ×, * DX = 0.0375 m, DT = 0.025 s. b. Data as in Fig. 12b. Solid line = theoretical solution by Madsen and White (1976). α_t, α_r by numerical solution: •, ▲ DX = 0.30 m, DT = 0.20 s; ○, △ DX = 0.15 m, DT = 0.10 s; ×, * DX = 0.075 m, DT = 0.05 s; □, ■ DX = 0.0375 m, DT = 0.025 s.

As seen from Fig. 14 the dissipation increases with increasing wave steepness. Furthermore it can be seen that using a coarse representation of the rubble-mound ($w/\Delta x = 1$) leads to an underestimation of the energy loss for the smallest wave steepnesses.

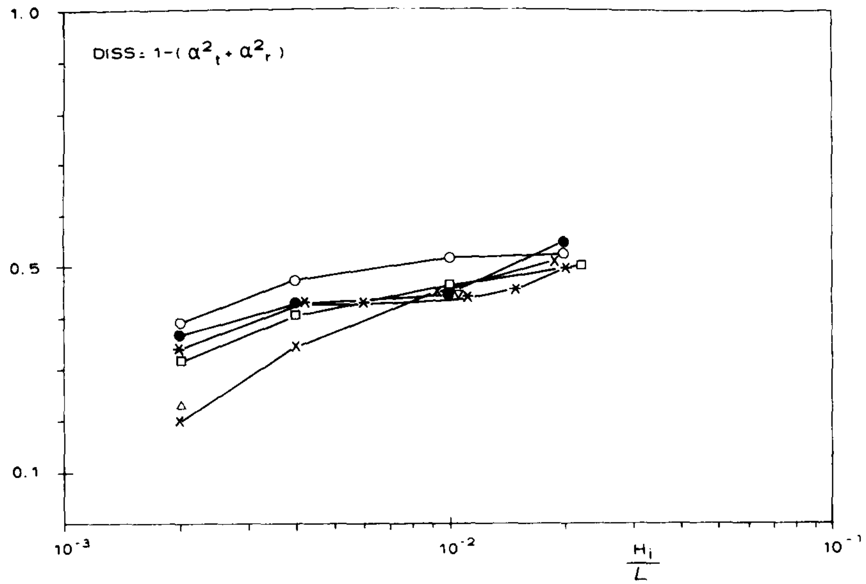

Fig. 14. Computed energy loss within the rubble-mound as a function of the wave steepness.

REFLECTION FROM A POROUS WAVE ABSORBER

In a wave absorber the core of the permeable breakwater is impervious and the transmission through the rubble-mound is eliminated. However, because of the energy loss inside the structure the reflections will only be partial.

Numerical model tests simulating wave absorbers have been carried out. The reflection coefficient is determined by Healy's formula as explained in the previous section.

In Fig. 15 the computed reflection coefficient is shown as a function of the width of the absorber divided by the wave length. Clearly, the absorber has to be quite long to be really efficient. The computational results are compared to an analytical solution made by Madsen (1983). This solution is based on linear shallow-water wave theory and is derived using a technique quite similar to that used by Madsen and White (1976) for transmission through rubble-mounds. The agreement with the numerical solution is seen to be very good, especially when α_R is not too high.

In Fig. 16 the reflection coefficient is shown as a function of the porosity. It turns out that we get the best absorption for a porosity as high as 0.95.

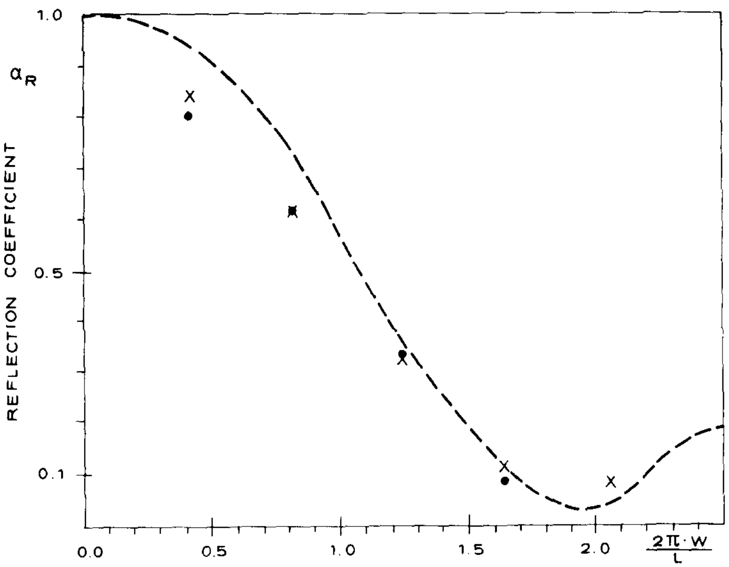

Fig. 15. The reflection from a wave absorber as a function of the width of the absorber divided by the wave length. Dashed line = theoretical solution; crosses = numerical model, DX = 15.5 m, DT = 1 s; circles = numerical model, DX = 7.75 m, DT = 0.5 s. T = 17.3 s, H = 1.74 m, h = 21 m, porosity = 0.95, diameter of grains = 0.2 m.

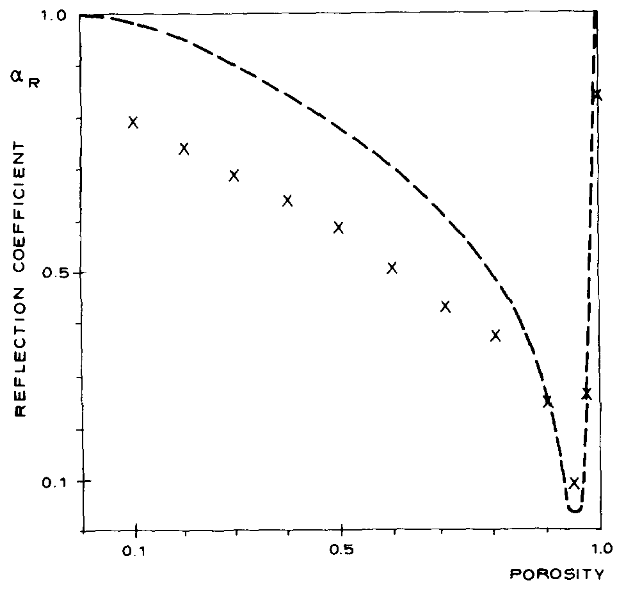

Fig. 16. The reflection from a wave absorber as a function of the porosity. Dashed line = theoretical solution; crosses = numerical solution, DX = 15.5 m, DT = 1 s. Basic parameters: diameter of stones, d = 0.2 m; width of the absorber, w = 77.5 m; wave period, T = 17.3 s; water depth, h = 21 m; wave height, H = 1.74 m.

This actually agrees with the measurements by Straub (1956), who used wire-mesh plates to obtain such high porosities. However, a quantitative comparison with the experimental results cannot be made as the absorbers used by Straub were not rectangular.

Instead the numerical solution is compared with the analytical solution by Madsen (1983). For small values of α_R the agreement is excellent but for α_R larger than 0.30 the comparison leaves something to be desired. However, the discrepancies for high values of α_R are due to non-linear effects which will have a considerable impact on the nodal value in the envelope of the surface elevations. The resulting reflection coefficient determined by Healy's linear formula will be lower than the true reflection coefficient. This is clearly illustrated by Fig. 16 where Healy's formula with a porosity equal to 1 leads to α_R equal to 0.84 instead of 1. On the other hand, Healy's formula will only be sensitive for small values of a_{min} (i.e. for high values of α_R) and the results appear to be reliable for small values of α_R.

Wave absorbers are of great importance in numerical modelling. For example if a certain area in a harbour is expected to have little or no influence on the wave conditions in the area of special interest, the first area can be deleted from the computations simply by combining a closed boundary with an absorbing filter layer. In this way a situation is simulated corresponding to full transmission of waves into the neglected areas from which no or little reflection is expected.

If full absorbtion is required at a boundary in the numerical model, other methods are more efficient than simulating porous wave absorbers (see Larsen and Dancy, 1983). This is due to the fact that reflection from porous wave absorbers is strongly nonlinear with respect to wave height and wave period (see Madsen, 1983) and a given absorber will only be efficient for a very narrow range of incoming wave characteristics.

CONCLUSIONS

A numerical model for simulation of the propagation of short waves has been compared with recognized analytical and experimental results for shoaling, refraction, diffraction and partial reflection. In general, the comparisons are entirely satisfactory, thus showing that the addition of the main Boussinesq terms to the normal conservation equations for nearly horizontal flow can be used to provide accurate simulations of short-wave phenomena. Elsewhere (Abbott et al., 1983), the importance of a consistent, third-order accurate finite-difference scheme for the solution of the equations is emphasized.

This paper proves that the application of numerical models (of the type described here) to the analysis and solution of practical engineering problems is justified. There are, of course, limitations on the ratios h/L, h/H and H/L (Abbott et al., 1983), but the range of validity is sufficient to cover most practical problems which can be characterized as studies of wave propagation over complex bathymetries where analytical solutions are not possible.

APPENDIX

The equations solved by the numerical model

The numerical model is based on the time-dependent vertically integrated Boussinesq equations conserving mass and momentum. The model is described in detail by Abbott et al. (1983). The equations are given below:

Continuity

$$n\frac{\partial \zeta}{\partial t}+\frac{\partial p}{\partial x}+\frac{\partial q}{\partial y}=0$$

x-momentum

$$n\frac{\partial p}{\partial t}+\frac{\partial}{\partial x}\left(\frac{p^2}{h}\right)+\frac{\partial}{\partial y}\left(\frac{pq}{h}\right)+n^2gh\frac{\partial \zeta}{\partial x}+n^2p\left(\alpha+\beta\sqrt{\frac{p^2}{h^2}+\frac{q^2}{h^2}}\right)$$

$$-\frac{p^2}{nh}\frac{\partial n}{\partial x}-\frac{pq}{nh}\frac{\partial n}{\partial y}=n\frac{Hh}{3}\left(\frac{\partial^3 p}{\partial x^2\partial t}+\frac{\partial^3 q}{\partial x\partial y\partial t}\right)$$

y-momentum

$$n\frac{\partial q}{\partial t}+\frac{\partial}{\partial y}\left(\frac{q^2}{h}\right)+\frac{\partial}{\partial x}\left(\frac{pq}{h}\right)+n^2gh\frac{\partial \zeta}{\partial y}+n^2q\left(\alpha+\beta\sqrt{\frac{p^2}{h^2}+\frac{q^2}{h^2}}\right)$$

$$-\frac{q^2}{nh}\frac{\partial n}{\partial y}-\frac{pq}{nh}\frac{\partial n}{\partial x}=n\frac{Hh}{3}\left(\frac{\partial^3 q}{\partial y^2\partial t}+\frac{\partial^3 p}{\partial x\partial y\partial t}\right)$$

where the following symbols are used:

Symbol	Description	Unit
$\zeta(x,y,t)$	water surface level above datum	(m)
$p(x,y,t)$	flux density in the x-direction	(m^3/s/m)
$q(x,y,t)$	flux density in the y-direction	(m^3/s/m)
$h(x,y,t)$	water depth	(m)
$H(x,y)$	still water depth	(m)
g	gravity	(m/s^2)
$n(x,y)$	porosity	
α	resistance coefficient for laminar flow in a porous media	
β	resistance coefficient for turbulent flow in a porous media	
x,y	space coordinates	(m)
t	time	(s)

REFERENCES

Abbott, M.B., Skovgaard, O. and Petersen, H.M., 1978. On the numerical modelling of short waves in shallow water. J. Hydraul. Res., 16(3).

Abbott, M.B., McCowan, A. and Warren, I.R., 1983. Extending the range of application of short-wave numerical models. In prep.

Engelund, F., 1953. On the laminar and turbulent flows of ground water through homogeneous sand. Trans. Danish Acad. Tech. Sci., 3(4).

Jonsson, I.G. and Carlsen, N.A., 1976. Experimental and theoretical investigations in a oscillatory rough turbulent boundary layer. J. Hydraul. Res., 14(1): 45—60.

Keulegan, G.H., 1973. Wave transmission through rock-structures. U.S. Army Engineer Waterways Experiments Station, Vicksburg, Research report no. H-73-1.

Larsen, J. and Dancy, H., 1983. Open boundaries in short wave simulation — a new approach. Coastal Eng., 7: 285—297.

Madsen, O.S. and White, S.M., 1976. Reflection and transmission characteristics of porous rubble-mound breakwaters. U.S. Army, Coastal Eng. Research Center, Miscellaneous report no. 76-5.

Madsen, P.A., 1983. Wave reflection from a vertical permeable wave absorber. Coastal Eng., 7: 381-396.

Shore Protection Manual, U.S. Army Coastal Engineering Research Center.

Singamsetti, S.R. and Wind, H.G., 1980. Characteristics of shoaling and breaking periodic waves normally incident to plane beaches of constant slope. Delft Hydraulics Laboratory, Report of Investigation, M1371.

Skovgaard, O. and Petersen, H.M., 1977. Refraction of cnoidal waves. Coastal Eng., 1: 43—61.

Straub, L.G., 1956. Experimental studies of wave filters and absorbers. St. Anthony Falls Hydraulic Laboratory, University of Minnesota, Project report no. 44.